

# Parallel Arrays of Sub-10 nm Aligned Germanium Nanofins from an “*In-situ*” Metal Oxide Hardmask using Directed Self-Assembly of Block Copolymers

Cian Cummins,<sup>†</sup> Anushka Gangnaik,<sup>¶</sup> Roisin A. Kelly,<sup>¶</sup> Alan J. Hydes,<sup>‡</sup> John O’Connell,<sup>¶</sup> Nikolay Petkov,<sup>¶</sup> Yordan M. Georgiev,<sup>¶</sup> Dipu Borah,<sup>†</sup> Justin D. Holmes<sup>¶§</sup> and Michael A. Morris<sup>†§\*</sup>

<sup>†</sup> Materials Research Group, Department of Chemistry and Tyndall National Institute, University College Cork, Cork, Ireland.

<sup>¶</sup> Materials Chemistry and Analysis Group, Department of Chemistry and Tyndall National Institute, University College Cork, Cork, Ireland.

<sup>‡</sup> SP&S, Tyndall National Institute, University College Cork, Cork, Ireland.

<sup>§</sup> Centre for Research on Adaptive Nanostructures and Nanodevices (CRANN/AMBER), Trinity College Dublin, Dublin, Ireland.

---

**ABSTRACT:** High-mobility materials and non-traditional device architectures are of key interest in the semiconductor industry because of the need to achieve higher computing speed and low power consumption. In this article, we present an integrated approach using directed self-assembly (DSA) of block copolymers (BCPs) to form aligned line-space features through graphoepitaxy on germanium on insulator (GeOI) substrates. Ge is an example of a high mobility material (III-V, II-VI) where the chemical activity of the surface and its composition sensitivity to etch processing offers considerable challenges in fabrication compared to silicon (Si). We believe the methods described here afford an opportunity to develop ultra-small dimension patterns from these important high-mobility materials. High quality metal oxide enhanced pattern transfer to Ge is demonstrated for the realization of nanofins with sub-10 nm feature size. Graphoepitaxial alignment of a poly(styrene)-*block*-poly(4-vinylpyridine) PS-*b*-P4VP BCP was achieved using pre-defined hydrogen silsesquioxane (HSQ) topography at a GeOI substrate. Subsequent impregnation of the aligned BCP templates with a salt precursor “*in-situ*” and simple processing was used to generate robust metal oxide nanowire (*e.g.* Fe<sub>3</sub>O<sub>4</sub>,  $\gamma$ -Al<sub>2</sub>O<sub>3</sub>, and HfO<sub>2</sub>) hardmask arrays. Optimized plasma based dry etching of the oxide modified substrate allowed the formation of high aspect ratio Ge nanofin features within the HSQ topographical structure. We believe the methodology developed has significant potential for high resolution device patterning of high mobility semiconductors. We envision that the aligned Ge nanofin arrays prepared here via graphoepitaxy might have application as a replacement channel material for complementary metal–oxide–semiconductor (CMOS) devices and integrated circuit (IC) technology. Furthermore, the low capital required to produce Ge nanostructures with DSA technology may be an attractive route to address technological and economic challenges facing the nanoelectronic and semiconductor industry.

---

With the inherent ability to form uniform periodically arranged nanoscale features, microphase separated BCPs have been under intense scrutiny as on-chip etch masks for patterning device relevant geometries (*e.g.* bends, junctions).<sup>1</sup> Microphase separation occurs due to the thermodynamic incompatibility between constituent blocks (A and B) of a di-BCP as represented by the dimensionless parameter,  $\chi$  (Flory-Huggins interaction parameter).<sup>2</sup> The degree of polymerization ( $N$ ) is the number of monomers forming the polymer chain and offers control of the periodicity of the resulting BCP microdomains.<sup>3</sup> Likewise, tailoring the volume fraction ( $f$ ) of respective blocks allows different morphologies to be attained, namely lamellae, gyroidal, cylindrical and finally spherical as  $f_A$  reduces from 0.5. With the need to achieve low feature sizes and pitches for ever decreasing technology nodes, “high  $\chi$ ” materials are required to allow a relatively high segregation strength  $\chi N$  ( $> 10.5$ ) as this enables ordered equilibrium morphologies to form.<sup>4</sup> DSA methodologies (namely chemoepitaxy and graphoepitaxy) over the past decade have primarily been demonstrated on silicon substrates using “first generation material” PS-*b*-PMMA BCP systems.<sup>5,6</sup> Demonstrations on 300 mm wafer scale pilot processes have recently been reported.<sup>7-9</sup> Two concerning issues for PS-*b*-PMMA are the minimum feature size attainable due to its’ low

$\chi$  (0.04)<sup>10</sup> and limited etch contrast between the organic blocks reducing pattern transfer fidelity.

In this regard, “high  $\chi$ ” BCP materials such as PS-*b*-PDMS ( $\chi \sim 0.26$ ), PS-*b*-P $x$ VPs ( $x = 2$  or 4, PS-*b*-P2VP  $\chi \sim 0.18$ ), and PS-*b*-PLA ( $\chi \sim 0.21$ ), are extremely attractive for reaching ultra-small features and have dominated recent literature.<sup>11-16</sup> Moreover, methodologies to selectively infiltrate and subsequently enhance microdomain etch contrast in neat self-assembled BCPs is now an area of considerable interest. In particular, sequential infiltration synthesis (*i.e.* SIS) has been documented for achieving high-aspect ratio silicon features from alumina infiltrated PS-*b*-PMMA.<sup>17-19</sup> Likewise, metal oxide inclusion has been reported to significantly enhance “activated” PS-*b*-PEO and PS-*b*-P4VP BCP systems for Si nanofeature fabrication.<sup>20-23</sup>

In order to extend the relentless dimensional scaling of semiconductor features (*i.e.* Moore’s Law) to the deep nanoscale regime ( $< 10$  nm), employing DSA of BCP nanopatterns has emerged as a cost-effective route to controllably fabricate device-relevant features on a wafer scale level. In parallel to research on the efficacy and integration of patterning technologies (*e.g.* DSA, extreme ultraviolet, electron-beam lithography, nanoimprint lithography), non-Si based materials such as graphene,<sup>24-28</sup> Ge,<sup>29,30</sup> carbon nanotubes,<sup>31</sup> and III-V<sup>32</sup> have

received significant attention for improved nanoelectronic device function mainly owing to their superior electrical properties. In particular, Ge has been suggested as a possible replacement material for MOSFETs to overcome future short channel effects which reduce device speed. Ge shares similar properties to its group IV neighbor Si, which makes a near term integration of a Si/Ge device possible or a complete replacement of Si channels viable in the future. Ge possesses a larger Bohr exciton radius ( $\sim 24.3$  nm) to Si ( $\sim 4.9$  nm)<sup>33</sup> consequently enhancing quantum effects, and Ge notably has higher electron and hole mobilities ( $3900$  cm<sup>2</sup>/V.s,  $1900$  cm<sup>2</sup>/V.s) than Si ( $1500$  cm<sup>2</sup>/V.s,  $450$  cm<sup>2</sup>/V.s)<sup>34</sup> thus potentially increasing electronic device speed. However, its brittleness, reactivity and unstable native oxides are serious areas of concern for device integration. If convenient process methods could be developed for the fabrication of high-mobility Ge devices using a GeOI platform, this would represent significant progress towards next-generation IC technologies.<sup>35</sup> The work reported here is a synergistic approach combining DSA of a high  $\chi$  BCP material and an inclusion methodology to pattern transfer to GeOI substrates. To the best of our knowledge, there are no reports to date on the graphoepitaxial alignment of a high  $\chi$  BCP and pattern transfer on Ge surfaces (bulk or GeOI). We have reported the thermal evaporation of Ge on porous BCP templates,<sup>36</sup> however the present work achieves well-defined structures of importance for current Si transistor architectures based on Fin-FET designs.

Scheme 1 displays the process flow used for the fabrication of the Ge nanofins reported here. Native Ge oxide on the GeOI surface was removed using a “green” approach of citric acid treatment based on previous work from these laboratories (Collins *et al.*<sup>37</sup>). The unstable native oxide of Ge is a major concern for its reintroduction to IC manufacture and the citric acid treatment is extremely effective for oxide removal and stabilization. The PS-*b*-P4VP BCP solution was spin-coated directly onto the passivated GeOI surface. Graphoepitaxially aligned self-assembled PS-*b*-P4VP line features were generated after solvent vapor annealing (SVA)<sup>38</sup> in a chloroform atmosphere. SVA of the 25 nm polymer thin film was carried out in an atmosphere of chloroform at room temperature for 2 hours to induce self-assembly. We have previously established a protocol for this cylinder forming PS-*b*-P4VP system with cylinder in-plane (C<sub>||</sub>) orientation achieved when employing non-selective solvent swelling conditions.<sup>23,39</sup>

Exposure of the self-assembled PS-*b*-P4VP patterns to hot ethanol resulted in porous channels that could be impregnated with metal oxide material. “Activation” (*i.e.* surface reconstruction)<sup>40,41</sup> of P4VP domains through selective block swelling in ethanol vapors was carried out at 50°C, and SEM characterization was employed to analyze films. Figure 1a shows a top-down SEM image of open area of an “activated” PS-*b*-P4VP BCP film displaying line-space features with high uniformity. Pitch and P4VP microdomain dimensions of the fingerprint patterns were measured at 32.45 nm and 8.63 nm respectively (see supporting information Figure S1) following SVA. Whilst hot ethanol immersion methods have been demonstrated to great effect,<sup>22,42</sup> we have observed film destruction as discussed in previous work.<sup>23</sup> Thus we have used hot ethanol vapors to create a near complete porous film. Parallel arrays of DSA of the “activated” PS-*b*-P4VP line-space features are displayed with high uniformity in Figure 1b-d. The SEM images show strict registration of the graphoepitaxially aligned “activated” PS-*b*-P4VP cylinder structures with the HSQ sidewall features. A total of 6, 7 and 11 P4VP C<sub>||</sub> features are visible within 224 nm, 265 nm, and 361 nm channel widths respectively. One should

note that larger periods of  $\sim 33$ - $35$  nm were formed in trench widths of 224 nm and 265 nm in comparison to  $\sim 32$  nm for open areas and larger channel widths. As we have outlined previously,<sup>39</sup> channel commensurability and SVA can alter microdomain feature size (especially at sidewalls) and thus we have employed larger channel widths here (*e.g.* 326 nm and 361 nm) to accommodate for added polymer expansion as a result of solvent uptake during annealing.

Following the controlled development of porous templates, fabrication of metal oxide nanowires mimicking the original polymer pattern was achieved. Here, as displayed in Figure 1e-h, Fe<sub>3</sub>O<sub>4</sub> nanowires on GeOI were enabled within HSQ prepatterns after spin coating of a low weight percentage iron nitrate ethanolic precursor onto the “activated” PS-*b*-P4VP template. An open area of Fe<sub>3</sub>O<sub>4</sub> nanowires on a GeOI substrate can be seen in the SEM image in Figure 1e. The high-resolution SEM image reveals nanowires that display a high level of regularity and uniformity. For pattern transfer lithography purposes, this is essential to avoid transferring any roughness or non-uniformity of the hardmask to the underlying substrate. The pitch and nanowire dimensions were comparable to the reconstructed films at 32.22 nm and 10.31 nm respectively. We elucidated the chemical composition of the iron nitrate precursor through XPS and SI Figure 2 shows confirmation of Fe<sub>3</sub>O<sub>4</sub> formation on GeOI. Figure 1f-h shows 6, 7, and 11 Fe<sub>3</sub>O<sub>4</sub> nanowires aligned within HSQ pre-patterns replicating the original “activated” PS-*b*-P4VP line-space features (Figure 1b-d). It can be seen that the precise nanowire feature positional accuracy and registration of Fe<sub>3</sub>O<sub>4</sub> material is consistent with aims to enhance current state-of-the-art IC patterning towards sub-10 nm features. The SEM images reveal that there is no P4VP wetting layer at the HSQ sidewalls allowing individually aligned nanowires to form. Substrate surface treatment or sidewall polymer brush modifications were not necessary to overcome interfacial effects. The neutrality of this cylinder forming PS-*b*-P4VP BCP system overcomes any previously outlined issues with selective wetting of polymer blocks at HSQ sidewalls such as PDMS containing BCPs in HSQ based prepatterns as described by Hobbs *et al.*<sup>43</sup> There is some indication of a Fe<sub>3</sub>O<sub>4</sub> wetting layer ( $\sim 2$  nm in thickness) after the inclusion step as displayed in the TEM image in Figure 1i. This extends across the channel base and the mesas (HSQ prepatterns). However, the nature of this layer remains uncertain. The possibility of forming such a regular wetting layer without forming cylinders would seem unlikely. There is also the likelihood of surface scattering effects that can lead to these apparent layers. We also note the possibility of the UV/O<sub>3</sub> treatment forming dense silica from the HSQ. The origin of this layer is under strict investigation. However, whatever its cause, it is clear that the etch procedure can “punch” through the residual surface layer. We also believe there is a residual HSQ layer at the substrate interface as discussed below. Note that the graphoepitaxial alignment of PS-*b*-P4VP and metal oxide inclusion was also carried out on bulk Ge substrates and large scale alignment were achieved with greater than 5 micron long features (see SI Figure S3).

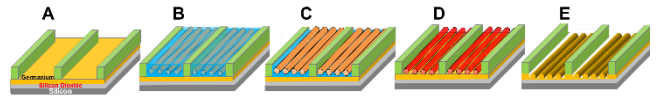
Figure 2b displays a top-down image of parallel arrays of 11 Ge nanofins within HSQ prepatterns following pattern transfer. A highly selective etch was employed using carbon tetrafluoride (CF<sub>4</sub>) gas only.<sup>44</sup> The Ge nanofins displayed in the TEM image in Figure 2c were fabricated after plasma etching of Ge for a total of 9 seconds. An initial shorter etch (3 seconds) revealed little removal of Ge material (see SI Figure S4). However on continued etching with CF<sub>4</sub>, aspect ratios of 1 : 3.5 were achieved within HSQ prepatterns as seen in the TEM data in

Figure 2c, d and e. Feature sizes and etch depths were measured at  $\sim 9$  nm and  $\sim 31$  nm respectively. The high dimensional control of the etch process is clearly evident. Interestingly, attempted chlorine based etch processes did not result in any etching of Ge. We believe this may be due to the residual HSQ material as seen in the TEM image in Figure 1i at the substrate interface between nanowire hardmask features and the Ge layer. Therefore,  $\text{Cl}_2$  plasma is unable to successfully etch the residual HSQ layer and pattern transfer the nanowire template to the Ge layer. In contrast,  $\text{CF}_4$  is well known to consume HSQ material<sup>43</sup> and thus rapidly etches the HSQ material at the substrate surface and enables Ge etching to take place. Further surface studies are required to gain insight into the mechanism. Overall, the issue was circumvented through employing alternative plasma etch chemistries allowing the creation of Ge nanofins. Also, whilst we demonstrate Ge nanostructures of application for Fin-FET based devices, further etching or thinner Ge thicknesses would enable the fabrication of Ge nanowires for other technological application.

In order to show the efficacy and robustness of the methodology outlined above we have employed aluminum and hafnium precursors as hardmask materials to pattern high-aspect ratio (1:6) Ge features on planar GeOI substrates. Figure 3a and b display top-down SEM images of alumina ( $\gamma\text{-Al}_2\text{O}_3$ ) and hafnia ( $\text{HfO}_2$ ) nanowire arrays with large scale coverage on GeOI substrates. The  $\gamma\text{-Al}_2\text{O}_3$  and  $\text{HfO}_2$  nanowires were fabricated using ethanolic based precursors as the  $\text{Fe}_3\text{O}_4$  nanowire hardmask arrays discussed above. High resolution XPS of Al  $2p$  and Hf  $4f$  are shown in insets in Figure 3a and b respectively confirming the presence of  $\gamma\text{-Al}_2\text{O}_3$  and  $\text{HfO}_2$ . The survey and high-resolution oxygen spectrum of both samples are shown and discussed further in SI Figure S5. The inclusion of semiconductor and high-k dielectric hardmask material in this simple reproducible process is advantageous for device processing considerations where industrial fabrication compatibility is essential. The spin-coating processes address scalability and throughput level that are paramount for high volume manufacturing (HVM) and very large scale integration (VLSI). Additionally, all steps for the fabrication of Ge nanofins were carried out at room temperature (290K). Ge etching using  $\text{CF}_4$  for 9 seconds was carried out for the pattern transfer of the  $\gamma\text{-Al}_2\text{O}_3$  and  $\text{HfO}_2$  hardmask nanowires to the underlying GeOI. Well-defined Ge nanofins were produced as shown from top-down SEM images in Figure 3c ( $\gamma\text{-Al}_2\text{O}_3$ ) and Figure 3d ( $\text{HfO}_2$ ) with good uniformity. Moreover, the cross-section SEM images displayed in Figure 3e and f reveal well-defined Ge nanofins from  $\gamma\text{-Al}_2\text{O}_3$  (Figure 3e) and  $\text{HfO}_2$  (Figure 3f) nanowire hardmasks. Clear evidence is revealed in the images of vertical and lateral dimensional control owing to the robustness of the etch mask and high selectivity of the dry etching process. The vertical profile of the Ge nanofins is also evident in the inset of each cross-section SEM views. Feature sizes were measured at 9 nm while depths were measured at 55 nm, *i.e.* an aspect ratio of 1:6.

In conclusion, we have presented a robust process flow for the fabrication of well-defined high-aspect ratio sub-10 nm Ge nanofin feature sizes with vertical and lateral dimensional control. The work demonstrates the level of accuracy in which a high  $\chi$  material could be used to template passivated GeOI substrate surfaces. Distinct and isolated  $\text{Fe}_3\text{O}_4$ ,  $\gamma\text{-Al}_2\text{O}_3$  and  $\text{HfO}_2$  nanowire hardmask arrays were also shown at GeOI substrate surfaces and were found to perform as excellent hardmasks for pattern transfer with each exhibiting similar efficacy. Highly selective dry etch procedures were employed to pattern transfer

the on-chip etch masks to the underlying GeOI substrate to generate Ge nanofins. More significantly, the self-assembly of PS-*b*-P4VP cylinders lying in-plane ( $\text{C}_{11}$ ), and selective P4VP infiltration with metal oxide material were all demonstrated with high reproducibility using a topographical DSA methodology. Graphoepitaxial HSQ prepatterns were fabricated using top-down electron-beam lithography to allow alignment and registration of cylinder forming PS-*b*-P4VP line-space features. Subsequent metal oxide nanowire fabrication and optimized etch time and chemistry enabled high-aspect ratio Ge nanofins to be achieved in graphoepitaxy trenches. Overall, the work emphasizes the possibility to realize next-generation electronic devices based on GeOI material through DSA of BCP technology for HVM and VLSI device designs.



**Scheme 1.** Process flow for fabrication of Ge nanofins. **A.** GeOI substrate after HSQ (green) prepattern development for graphoepitaxy. **B.** PS-*b*-P4VP film after solvent vapor annealing producing aligned P4VP cylinders parallel to substrate. **C.** Activated PS-*b*-P4VP film after ethanol vapor exposure. **D.** Metal oxide nanowire hardmask after spin coating metal-salt precursor and successful metal ion oxidation and polymer template removal via UV/ $\text{O}_3$ . **E.** Aligned Ge nanofin fabrication following pattern transfer of hardmask.

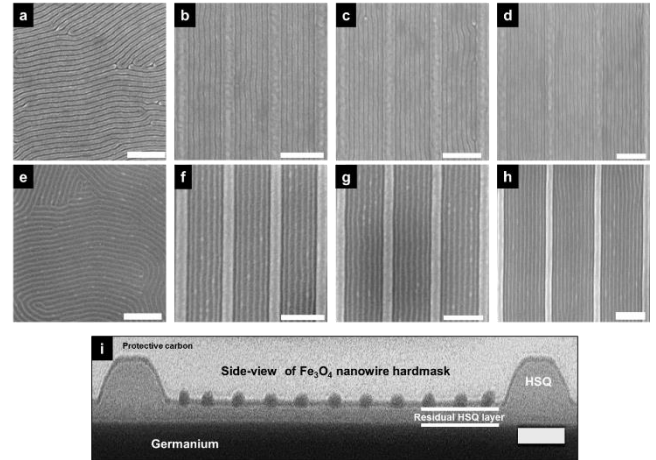


**Figure 1.** Top-down SEM images of (a) open area of porous “activated” PS-*b*-P4VP films. (b) – (d) display graphoepitaxial alignment of “activated” features in HSQ prepatterns of 224 nm, 265 nm and 361 nm channel widths respectively. SEM images in (e)-(h) show corresponding  $\text{Fe}_3\text{O}_4$  nanowire hardmask features after metal oxide inclusion in open areas and within HSQ prepatterns. All scale bars represent 250 nm. (i) Cross-section TEM image of  $\text{Fe}_3\text{O}_4$  nanowire hardmask features in HSQ prepattern of 361 nm channel widths [*i.e.* image (h)]. Scale bar is 50 nm. Note there is evidence of a residual HSQ layer (between white lines). There is also possible evidence of hardened HSQ between  $\text{Fe}_3\text{O}_4$  nanowires and along surface of HSQ material.

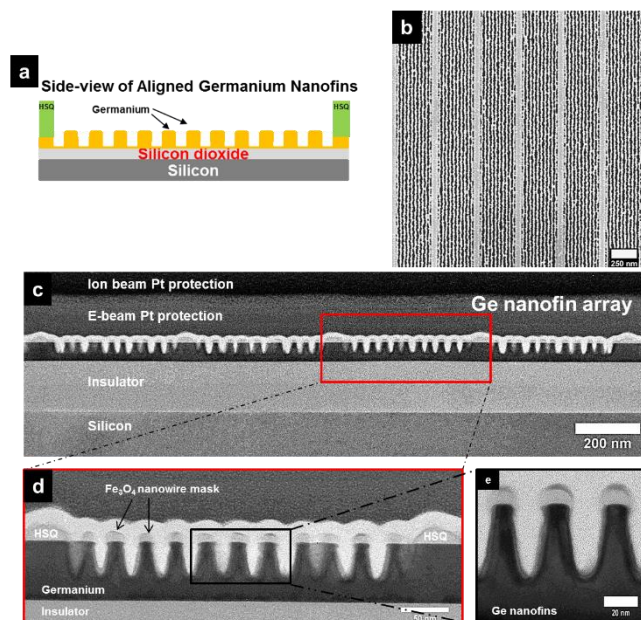


**Figure 2.** (a) Shows cross-section profile of aligned Ge nanofins following pattern transfer. (b) top-down SEM image of parallel arrays of pattern transferred Ge nanofins in channel widths of 361 nm. (c)-(e) Low resolution and high-resolution TEM images of graphoepitaxially aligned Ge nanofin structures corresponding to (b).

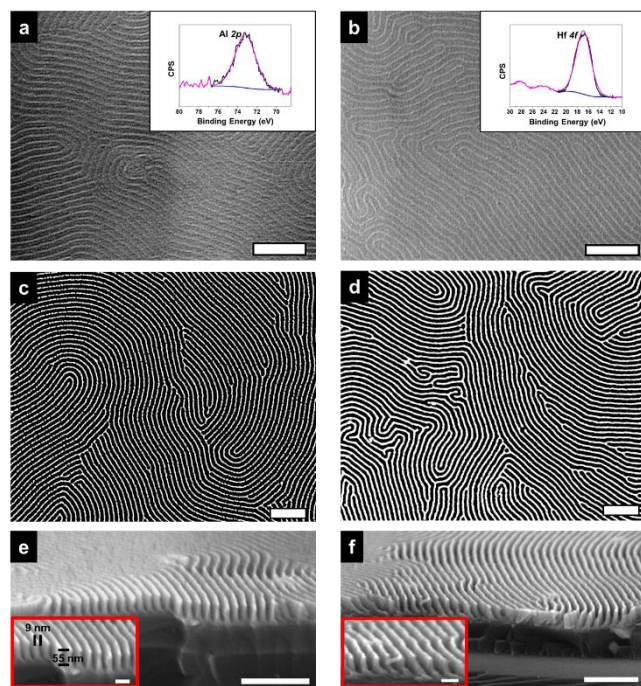


**Figure 3.** Top-down SEM images of  $\gamma$ -Al<sub>2</sub>O<sub>3</sub> nanowire (a) and HfO<sub>2</sub> nanowire (b) arrays following metal-salt inclusion process. Insets in (a) and (b) show high resolution XPS scans for Al 2p and Hf 4f peaks. Top-down SEM of Ge nanofins following pattern transfer with (c)  $\gamma$ -Al<sub>2</sub>O<sub>3</sub> nanowire hardmask and (d) HfO<sub>2</sub> nanowire hardmask. Corresponding cross-section SEM images in (e) and (f) reveal high uniformity of Ge nanofin structures. Main scale bars represent 250 nm whilst insets are 50 nm.

## ASSOCIATED CONTENT

**Supporting Information:** This information is available free of charge via the Internet at <http://pubs.acs.org>.

Materials used and experimental details, S1. Feature size and pitch calculations, S2. XPS data of Fe<sub>3</sub>O<sub>4</sub>, S3. SEM images of “activated” features in HSQ pre-patterns, S4. SEM images of Fe<sub>3</sub>O<sub>4</sub> nanowires following brief CF<sub>4</sub> etch, S5. XPS data of  $\gamma$ -Al<sub>2</sub>O<sub>3</sub> and HfO<sub>2</sub>.

## AUTHOR INFORMATION

### Corresponding Author

\* Michael A. Morris, E-mail: [m.morris@ucc.ie](mailto:m.morris@ucc.ie)

### Author Contributions

The manuscript was written through contributions of all authors. All authors have given approval to the final version of the manuscript.

## ACKNOWLEDGMENT

Funding Sources: The authors gratefully acknowledge Science Foundation Ireland (SFI) (Grant number 09/IN.1/602) CSET/CRANN and LAMAND NMP FP7 grant for funding this project.

## REFERENCES

1. Stoykovich, M. P.; Kang, H.; Daoulas, K. C.; Liu, G.; Liu, C.-C.; de Pablo, J. J.; Müller, M.; Nealey, P. F. Directed Self-Assembly of Block Copolymers for Nanolithography: Fabrication of Isolated Features and Essential Integrated Circuit Geometries. *ACS Nano* **2007**, *1*, 168-175.
2. Mai, Y.; Eisenberg, A. Self-assembly of block copolymers. *Chemical Society Reviews* **2012**, *41* (18), 5969-5985.
3. Schacher, F. H.; Rupar, P. A.; Manners, I. Functional block copolymers: Nanostructured materials with emerging applications. *Angew. Chem. Int. Ed.* **2012**, *51*, 7898-7921.
4. Koo, K.; Ahn, H.; Kim, S.-W.; Ryu, D. Y.; Russell, T. P. Directed self-assembly of block copolymers in the extreme: guiding microdomains from the small to the large. *Soft Matter* **2013**, *9*, 9059-9071.
5. Stoykovich, M. P.; Müller, M.; Kim, S. O.; Solak, H. H.; Edwards, E. W.; De Pablo, J. J.; Nealey, P. F. Materials Science: Directed assembly of block copolymer blends into nonregular device-oriented structures. *Science* **2005**, *308*, 1442-1446.
6. Farrell, R. A.; Kinahan, N. T.; Hansel, S.; Stuen, K. O.; Petkov, N.; Shaw, M. T.; West, L. E.; Djara, V.; Dunne, R. J.; Varona, O. G.; Gleeson, P. G.; Jung, S. J.; Kim, H. Y.; Kolešnik, M. M.; Lutz, T.; Murray, C. P.; Holmes, J. D.; Nealey, P. F.; Duesberg, G. S.; Krstić, V.; Morris, M. A. Large-scale parallel arrays of silicon nanowires via block copolymer directed self-assembly. *Nanoscale* **2012**, *4*, 3228-3236.
7. Delgadillo, P. A. R.; Gronheid, R.; Thode, C. J.; Wu, H.; Cao, Y.; Neisser, M.; Somervell, M.; Nafus, K.; Nealey, P. F. Implementation of a chemo-epitaxy flow for directed self-assembly on 300-mm wafer processing equipment. *J Micro Nanolithogr MEMS MOEMS* **2012**, *11*, 031302.
8. Liu, C.-C.; Estrada-Raygoza, I. C.; Abdallah, J.; Holmes, S.; Yin, Y.; Schepis, A.; Cicoria, M.; Hetzer, D.; Tsai, H.; Guillorn, M.; Tjio, M.; Cheng, J.; Somervell, M.; Colburn, M. Directed self-assembly process implementation in a 300mm pilot line environment. *Proc. SPIE.* 2013; 86801G.
9. Isabelle, S.; Raluca, T.; Ahmed, G.; Maxime, A.; Karine, J.; Gaëlle, C.-M.; Patricia Pimenta, B.; Xavier, C.; Jérôme, B.;

- Xavier, B.; Sylvain, M.; Christophe, N.; Gilles, C.; Sébastien, B.; Masaya, A.; Charles, P. Contact hole shrink by directed self-assembly: Process integration and stability monitored on 300 nm pilot line. *Jpn. J. Appl. Phys.* **2014**, *53*, 06JC05.
10. Cheng, H.-H.; Keen, I.; Yu, A.; Chuang, Y.-M.; Blakey, I.; Jack, K. S.; Leeson, M. J.; Younkin, T. R.; Whittaker, A. K. EUVL compatible LER solutions using functional block copolymers, *Proc. SPIE* **2012**; pp 832310.
  11. Gotrik, K. W.; Ross, C. A. Solvothermal Annealing of Block Copolymer Thin Films. *Nano Letters* **2013**, *13*, 5117-5122.
  12. Chai, J.; Wang, D.; Fan, X.; Buriak, J. M. Assembly of aligned linear metallic patterns on silicon. *Nat. Nano.* **2007**, *2*, 500-506.
  13. Chai, J.; Buriak, J. M. Using Cylindrical Domains of Block Copolymers To Self-Assemble and Align Metallic Nanowires. *ACS Nano* **2008**, *2*, 489-501.
  14. Gu, X.; Liu, Z.; Gunkel, I.; Chourou, S. T.; Hong, S. W.; Olynick, D. L.; Russell, T. P. High Aspect Ratio Sub-15 nm Silicon Trenches From Block Copolymer Templates. *Adv. Mater.* **2012**, *24*, 5688-5694.
  15. Mokarian-Tabari, P.; Cummins, C.; Rasappa, S.; Simao, C.; Sotomayor Torres, C. M.; Holmes, J. D.; Morris, M. A. Study of the Kinetics and Mechanism of Rapid Self-Assembly in Block Copolymer Thin Films during Solvo-Microwave Annealing. *Langmuir* **2014**, *30*, 10728-10739.
  16. Keen, I.; Cheng, H.-H.; Yu, A.; Jack, K. S.; Younkin, T. R.; Leeson, M. J.; Whittaker, A. K.; Blakey, I. Behavior of Lamellar Forming Block Copolymers under Nanoconfinement: Implications for Topography Directed Self-Assembly of Sub-10 nm Structures. *Macromolecules* **2013**, *47*, 276-283.
  17. Tseng, Y.-C.; Peng, Q.; Ocola, L. E.; Elam, J. W.; Darling, S. B. Enhanced Block Copolymer Lithography Using Sequential Infiltration Synthesis. *J. Phys. Chem. C* **2011**, *115*, 17725-17729.
  18. Johnston, D. E.; Lu, M.; Black, C. T. Plasma etch transfer of self-assembled polymer patterns. *J Micro Nanolithogr MEMS MOEMS* **2012**, *11*, 031306.
  19. Ruiz, R.; Wan, L.; Lille, J.; Patel, K. C.; Dobisz, E.; Johnston, D. E.; Kisslinger, K.; Black, C. T. Image quality and pattern transfer in directed self assembly with block-selective atomic layer deposition. *J. Vac. Sci. Technol. B* **2012**, *30*, 06F202.
  20. Ghoshal, T.; Senthamaraiannan, R.; Shaw, M. T.; Holmes, J. D.; Morris, M. A. "In situ" hard mask materials: a new methodology for creation of vertical silicon nanopillar and nanowire arrays. *Nanoscale* **2012**, *4*, 7743-7750.
  21. Cummins, C.; Borah, D.; Rasappa, S.; Chaudhari, A.; Ghoshal, T.; O'Driscoll, B. M. D.; Carolan, P.; Petkov, N.; Holmes, J. D.; Morris, M. A. Self-assembly of polystyrene-*block*-poly(4-vinylpyridine) block copolymer on molecularly functionalized silicon substrates: fabrication of inorganic nanostructured etchmask for lithographic use. *J. Mater. Chem. C* **2013**, *1*, 7941-7951.
  22. Ghoshal, T.; Senthamaraiannan, R.; Shaw, M. T.; Holmes, J. D.; Morris, M. A. Fabrication of ordered, large scale, horizontally-aligned Si nanowire arrays based on an in situ hard mask block copolymer approach. *Adv. Mater.* **2014**, *26*, 1207-1216.
  23. Cummins, C.; Gangnaik, A.; Kelly, R. A.; Borah, D.; O'Connell, J.; Petkov, N.; Georgiev, Y. M.; Holmes, J. D.; Morris, M. A. Aligned silicon nanofins via the directed self-assembly of PS-*b*-P4VP block copolymer and metal oxide enhanced pattern transfer. *Nanoscale* **2015**, *7*, 6712-6721.
  24. Schwierz, F. Graphene transistors. *Nat. Nano.* **2010**, *5*, 487-496.
  25. Liang, X.; Wi, S. Transport Characteristics of Multichannel Transistors Made from Densely Aligned Sub-10 nm Half-Pitch Graphene Nanoribbons. *ACS Nano* **2012**, *6*, 9700-9710.
  26. Liu, G.; Wu, Y.; Lin, Y.-M.; Farmer, D. B.; Ott, J. A.; Bruley, J.; Grill, A.; Avouris, P.; Pfeiffer, D.; Balandin, A. A.; Dimitrakopoulos, C. Epitaxial Graphene Nanoribbon Array Fabrication Using BCP-Assisted Nanolithography. *ACS Nano* **2012**, *6*, 6786-6792.
  27. Son, J. G.; Son, M.; Moon, K.-J.; Lee, B. H.; Myoung, J.-M.; Strano, M. S.; Ham, M.-H.; Ross, C. A. Sub-10 nm Graphene Nanoribbon Array Field-Effect Transistors Fabricated by Block Copolymer Lithography. *Adv. Mater.* **2013**, *25*, 4723-4728.
  28. Seokhan, P.; Je Moon, Y.; Uday Narayan, M.; Hyoung-Seok, M.; Hyeong Min, J.; Sang Ouk, K. Device-oriented graphene nanopatterning by mussel-inspired directed block copolymer self-assembly. *Nanotechnology* **2014**, *25*, 014008.
  29. O'Regan, C.; Biswas, S.; Petkov, N.; Holmes, J. D. Recent advances in the growth of germanium nanowires: synthesis, growth dynamics and morphology control. *J. Mater. Chem. C* **2014**, *2*, 14-33.
  30. Zhang, J.; Gao, Y.; Hanrath, T.; Korgel, B. A.; Buriak, J. M. Block copolymer mediated deposition of metal nanoparticles on germanium nanowires. *Chem. Commun.* **2007**, 1438-1440.
  31. Baughman, R. H.; Zakhidov, A. A.; de Heer, W. A. Carbon Nanotubes--the Route Toward Applications. *Science* **2002**, *297*, 787-792.
  32. Monemar, B. III-V nitrides - important future electronic materials. *J. Mater. Sci. Mater. Electron* **1999**, *10*, 227-254.
  33. Gu, G.; Burghard, M.; Kim, G. T.; Düsberg, G. S.; Chiu, P. W.; Krstic, V.; Roth, S.; Han, W. Q. Growth and electrical transport of germanium nanowires. *J. Appl. Phys.* **2001**, *90*, 5747-5751.
  34. Drinek, V.; Fajgar, R.; Klementova, M.; Subrt, J. Deposition of Germanium Nanowires from Digermane Precursor: Influence of the Substrate Pretreatment. In *Eurocvd 17 / Cvd 17*, Swihart, M. T.; Barreca, D.; Adomaitis, R. A.; Worhoff, K., Eds. 2009; Vol. 25, pp 1015-1022.
  35. Akatsu, T.; Deguet, C.; Sanchez, L.; Allibert, F.; Rouchon, D.; Signamarcheix, T.; Richtarch, C.; Boussagol, A.; Loup, V.; Mazen, F.; Hartmann, J.-M.; Campidelli, Y.; Clavelier, L.; Letertre, F.; Kernevez, N.; Mazure, C. Germanium-on-insulator (GeOI) substrates—A novel engineered substrate for future high performance devices. *Mater. Sci. Semicond. Process.* **2006**, *9*, 444-448.
  36. Rasappa, S.; Borah, D.; Senthamaraiannan, R.; Faulkner, C. C.; Wang, J. J.; Holmes, J. D.; Morris, M. A. Fabrication of Germanium Nanowire Arrays by Block Copolymer Lithography. *Sci. Adv. Mater.* **2013**, *5*, 782-787.
  37. Collins, G.; Aureau, D.; Holmes, J. D.; Etcheberry, A.; O'Dwyer, C. Germanium Oxide Removal by Citric Acid and Thiol Passivation from Citric Acid-Terminated Ge(100). *Langmuir* **2014**, *30*, 14123-14127.
  38. Sinturel, C.; Vayer, M.; Morris, M.; Hillmyer, M. A. Solvent Vapor Annealing of Block Polymer Thin Films. *Macromolecules* **2013**, *46*, 5399-5415.
  39. Cummins, C.; Kelly, R. A.; Gangnaik, A.; Georgiev, Y. M.; Petkov, N.; Holmes, J. D.; Morris, M. A. Solvent Vapor Annealing of Block Copolymers in Confined Topographies: Commensurability Considerations for Nanolithography. *Macromol. Rapid Commun.* **2015**, *36*, 762-767.
  40. Park, S.; Kim, B.; Wang, J. Y.; Russell, T. P. Fabrication of Highly Ordered Silicon Oxide Dots and Stripes from Block Copolymer Thin Films. *Adv. Mater.* **2008**, *20*, 681-685.
  41. Park, S.; Wang, J.-Y.; Kim, B.; Xu, J.; Russell, T. P. A Simple Route to Highly Oriented and Ordered Nanoporous Block Copolymer Templates. *ACS Nano* **2008**, *2*, 766-772.
  42. Yin, J.; Yao, X.; Liou, J.-Y.; Sun, W.; Sun, Y.-S.; Wang, Y. Membranes with Highly Ordered Straight Nanopores by Selective Swelling of Fast Perpendicularly Aligned Block Copolymers. *ACS Nano* **2013**, *7*, 9961-9974.

43. Hobbs, R. G.; Farrell, R. A.; Bolger, C. T.; Kelly, R. A.; Morris, M. A.; Petkov, N.; Holmes, J. D. Selective Sidewall Wetting of Polymer Blocks in Hydrogen Silsesquioxane Directed Self-Assembly of PS-*b*-PDMS. *ACS Appl. Mater. Interfaces* **2012**, *4*, 4637-4642.

44. Shim, K.-H.; Yang, H. Y.; Kil, Y.-H.; Yang, H. D.; Yang, J.-H.; Hong, W.-K.; Kang, S.; Jeong, T. S.; Kim, T. S. Nanoscale dry etching of germanium by using inductively coupled CF<sub>4</sub> plasma. *Electron Mater Lett* **2012**, *8*, 423-428.

---

Authors are required to submit a graphic entry for the Table of Contents (TOC) that, in conjunction with the manuscript title, should give the reader a representative idea of one of the following: A key structure, reaction, equation, concept, or theorem, etc., that is discussed in the manuscript. Consult the journal's Instructions for Authors for TOC graphic specifications.

---

Insert Table of Contents artwork here

---

